8th International Symposium on Superalloy 718 and Derivatives
Edited by: Eric Ott, Anthony Banik, Xingbo Liu, Ian Dempster, Karl Heck, Joel Andersson, Jon Groh, Tim Gabb, Randy Helmink, and Agnieszka Wusatowska-Sarnek
TMS (The Minerals, Metals & Materials Society), 2014

OXIDATION BEHAVIOR OF HAYNES® 282® IN STEAM AT 750°C

Liying Tang, Rongcan Zhou, Yan Guo, Bohan Wang, Shufang Hou

Xi'an Thermal Power Research Institute Co. Ltd.
136 Xingqing Road; Xi'an, Shaanxi, 710032, PRC

Keywords: Steam, Oxidation, Haynes 282, Kinetics, TiO_2

Abstract

Advanced ultra-supercritical (A-USC) power plants operate at steam temperatures of 700°C and above are the development trend of clean coal power generation technology. Haynes® 282® has gained great attention as one of candidate materials for A-USC power units. In this paper the oxidation behavior of Haynes® 282® in steam at 750°C for up to 2000h was investigated. The oxidation kinetics was obtained and the microstructure, constitution and element distribution of the oxide scales and the subsurface zones was studied. The results indicated that the oxide scale of Haynes® 282® in steam was composed of a continuous external layer and an internal subscale. The external scale was essentially composed of Cr_2O_3 and TiO_2 but the internal oxide was mainly Al_2O_3. TiO_2 grains grew up and were connected with each other during the oxidation, and the fractional volume of TiO_2 increased obviously with oxidation time. Ti was enriched both at the gas/solid and oxide/metal interfaces. TiO_2 is believed to be harmful to the oxidation resistance of Haynes® 282® in steam due to its promotion of the adsorption and decomposition of H_2O as well as the higher diffusion rate of H in it.

Introduction

The environmental restrictions on the fossil power generation plants require further increased steam temperature and pressure. 700°C advanced ultra-supercritical (A-USC) power generation technology is the direction of research and development of fossil power plants [1-6]. At steam temperatures above 700°C, the ferritic and austenitic heat resistant steel can't meet with the strength requirements for superheater, reheater and pipes. Ni-based superalloys such as Inconel® 740H, Alloy 617B and Haynes® 282® will be required.

Haynes® 282® is a newly developed γ′ strengthened Ni-based superalloy, which allows for service temperature ranging from 649 to 927°C [7–14] and has been widely used for aero engine and gas turbine applications due to a combination of exceptional creep strength, good thermal stability and superior fabricability. Haynes International Inc. reported the microstructure, mechanical properties and welding performance [7–14]. EPRI has also reported the effect of prior aging treatments on the creep properties of Haynes® 282® [15]. Some papers focused on the oxidation and corrosion properties. For example, the thicknesses of oxide scale of Haynes® 282® after oxidation in flow air at 871°C, 927°C and 982°C for 1008 hours were investigated [14]. The corrosion resistance of Haynes® 282® in the fuel combustion simulation environment at 871°C for 1000 hours was also revealed [14]. Water vapor is known to considerably accelerate oxidation rates of high temperature alloys. Cycle oxidation testing was carried at 760°C and 871°C in air + 10% H_2O for 1,008 hours by Vinay P. Deodeshmukh and Nacéra Sabrina Meck [16]. The oxidation mechanism of metals in steam is very different from that in air containing H_2O due to the obvious lower oxygen partial pressure. Hence the oxidation resistance in steam is

an important property for materials used in A-USC power units. Up to now, there are rather limited data on the oxidation resistance of Haynes® 282® in steam.

In this paper the oxidation behavior of Haynes® 282® in steam at 750°C for up to 2000 hours was investigated. The purpose is to evaluate the steam oxidation resistance of Haynes® 282® and the growth mechanism of the oxide scale in steam will be discussed.

Materials and methods

Materials for the steam oxidation were commercial tubes of Haynes® 282® with dimensions of Φ38×8.8mm, whose average grain size was ASTM 3. The chemical composition is shown in Table 1. The tubes were cut and machined into specimens with dimension of 25×12×3mm. The roughness was nearly Ra 0.8μm. The specimens were ultrasonically cleaned with acetone and dried for at least 12 hours before the oxidation test.

The schematic diagram of the steam oxidation test apparatus is shown in Figure 1. The feed water was deionized and deaerated until dissolved oxygen content was less than 20ppb. The specimens were under the protection of argon in the process of startup and shutdown.
The oxidation test was carried out at 750°C for up to 2000h. The specimens were respectively taken out at 100 h, 300 h, 600 h, 1000 h and 2000 h intervals, and were weighed.

The phase structure of the oxide was identified with a SHIMADZU 7000-type X-ray diffractmeter (XRD). The microstructure and composition of the surface and the cross section of the oxide scale was analyzed with an FEI QUANTA-400 scanning electron microscope (SEM) and an Oxford INCA X-ray spectrometer (EDS).

Table 1 Chemical composition of Haynes® 282® (wt. %)

Elements	C	Si	Mn	Al	Ti	Co	S	P	Fe	Cr	Mo	Nb+Ta	Cu	Ni
weight percentage	0.07	0.14	0.04	1.4	2.1	10.2	0.0009	0.008	0.93	19.91	8.5	0.035	0.010	Bal.

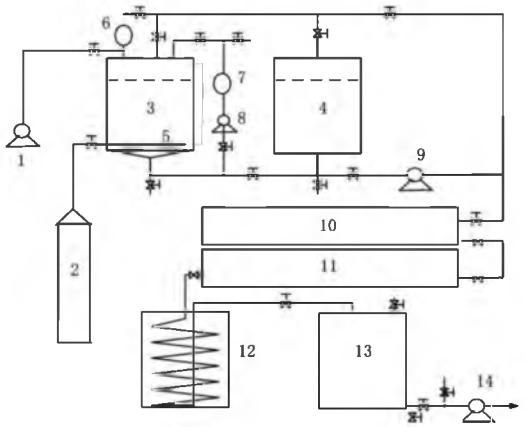

Figure 1 Schematic diagram of high-temperature steam oxidation test rig
1-vacuum pump; 2-high purity argon; 3-water tank A; 4-water tank B; 5-argon tube; 6- pressure gauge; 7-oxygen content meter; 8- water pump; 9- metering pump; 10- preheating furnace; 11-specimen furnace; 12-condenser; 13-water tank C; 14- water pump.

Results and discussion

The weights of the specimens were measured and the mass gains at different times were calculated. The oxidation kinetic curve is plotted in Figure 2 in term of the average mass gain against oxidation time. The fitting formula was as follows:

$$\Delta m^{2.57566}=0.0006t \quad (1)$$

Where Δm is mass gain (mg/cm^2); t is oxidation time (hours). It is clear that the oxidation kinetics obeys parabolic rule, indicating that the oxidation rate was controlled by the diffusion rate of the element through the oxide scale. The mass gain in steam at 750°C for 1000h was nearly 4 times higher than that of oxidation testing in air+10%H_2O at 760°C for 1,008 hours [16], indicating corrosion was more severe in steam than in air containing water vapor.

The XRD spectra of the oxide scale of Haynes® 282® after oxidation for 2000 hours is shown in Figure 3. The main oxide phases were TiO_2 and Cr_2O_3. The diffraction peaks of the base metals were obvious, indicating the oxide scales were fairly thin.

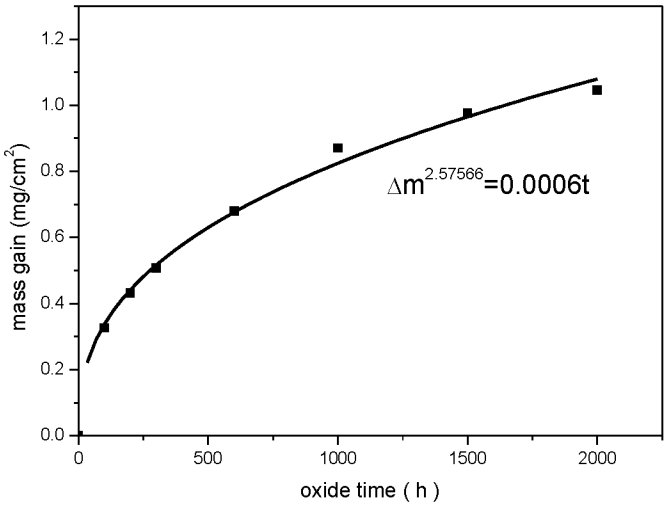

Figure 2 Oxidation kinetics of Haynes® 282®

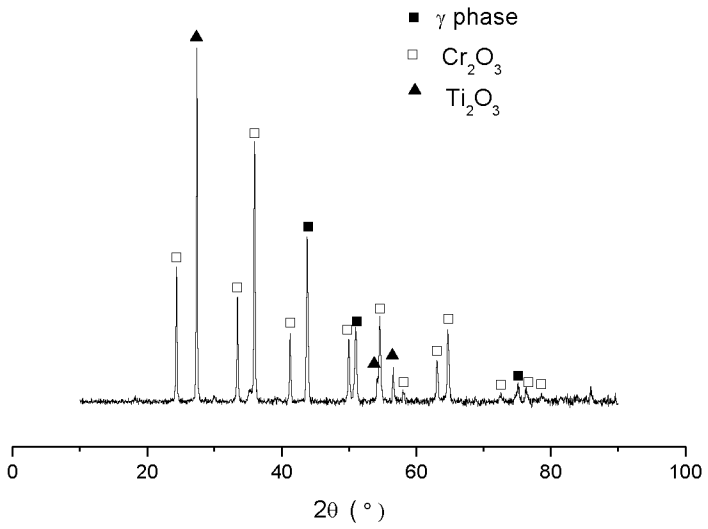

Figure 3 XRD spectra of the oxide scale after steam oxidation test at 750°C for 2000 h

Particles with sizes of 0.5~1μm were observed on the scale of Haynes® 282® after oxidation for 100 hours (see Figure 4 (a)). The particles grew up and connected with each other with an increase of oxidation time, which were identified to be TiO_2 by means of EDS analysis (see 1000h-A in Table 2). The oxide as marked with "B" in Figure 4 (c) was considered to be mostly Cr_2O_3 due to the fairly high Cr content. No spallation was found in all the specimens.

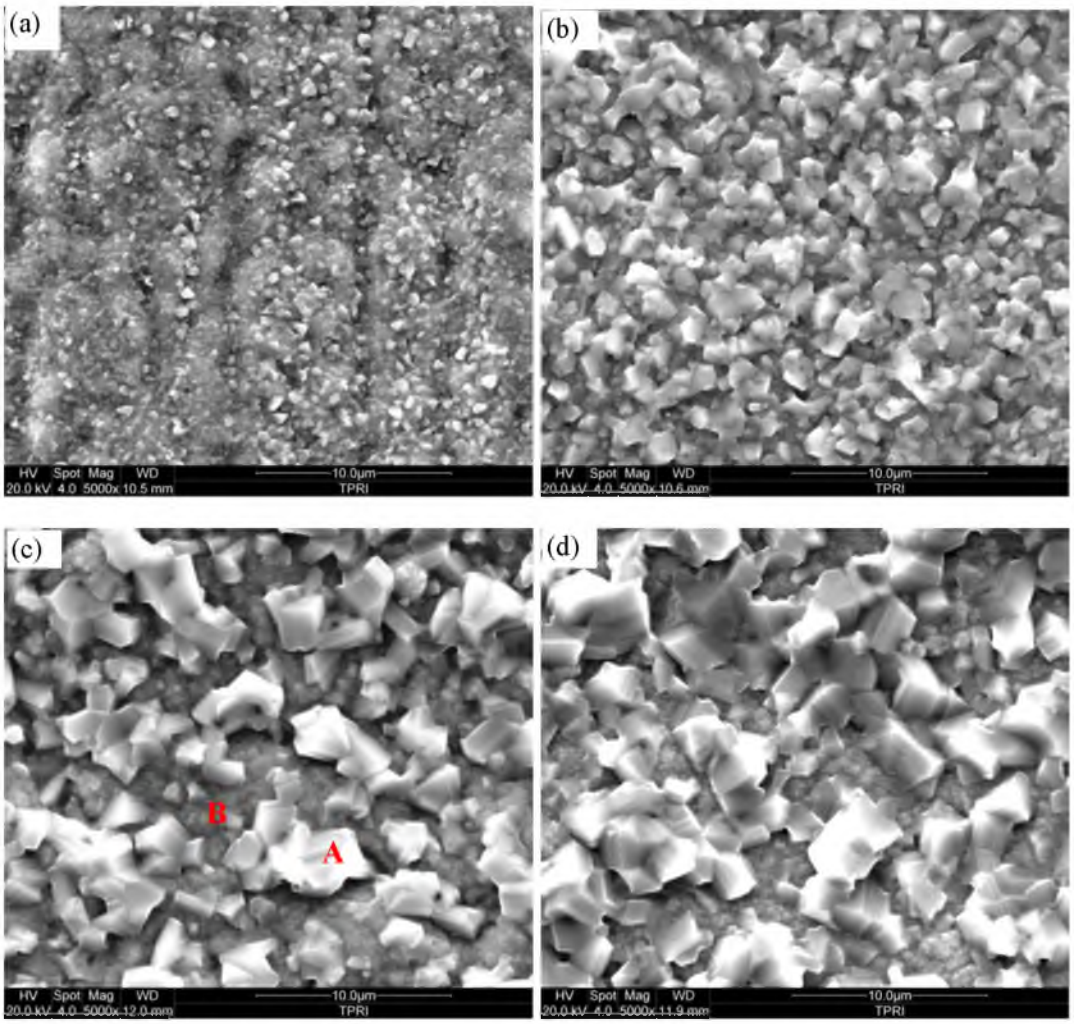

Figure 4 SEM morphologies of the specimen surface after oxidation in steam for different time
(a) 100 hours (b) 300 hours (c) 1000 hours (d) 2000 hours

The average compositions of the oxide scale surface after oxidation in steam at 750°C for different time are shown in Table 2. It can be obviously observed that the Ti content increased, whereas the Cr content decreased with oxidation time, suggesting the TiO_2 content in the oxide scale increased distinctly.

Table 2 Composition of the oxide scale surface after oxidation in steam at 750°C（wt%）

Oxidation time	O	Al	Ti	Cr	Mn	Fe	Co	Ni
100h- Average	27.51	0.16	**10.56**	**57.61**	0.92	0.30	0.60	2.34
1000h- Average	32.98	/	**14.18**	**49.19**	1.40	0.47	0.84	0.93
2000h- Average	33.86	/	**20.99**	**42.46**	1.40	0.62	/	0.66
1000h-A	46.38	/	**29.85**	**14.28**	4.82	1.26	1.53	1.88
1000h-B	30.38	/	**5.88**	**60.24**	1.12	0.50	0.82	1.06

Cross sectional images of the oxide scales after oxidation at 750°C are shown in Figure 5. It can be seen that the oxide scale was composed of an external layer and an internal oxidation subscale. The internal oxide was net-like and along grain boundaries and sub-grain boundaries. The external scale thicknesses and the internal penetration depths were measured and the oxidation kinetic curves were plotted in Figure 6 (a). It is clear that the external scale thickness and the internal penetration depth both increased with oxidation time, which basically follows the parabola law.

We defined two parameters as follows:

$$f_i = \frac{\text{internal penetration depth}}{\text{external scale thickness} + \text{internal penetration depth}} \tag{2}$$

$$f_e = \frac{\text{external scale thickness}}{\text{external scale thickness} + \text{internal penetration depth}} \tag{3}$$

Figure 6 (b) shows the relationship between the two parameters and oxidation time. It can be clearly seen that f_e increased but f_i decreased with oxidation time, indicating the diffusion rate of oxygen through the external oxide scale decreased.

The element distribution after oxidation at 750°C for 2000 h are given in Figure 7, and the EDS line scanning (position in Figure 5 (c)) results are shown in Figure 8. It is clear that the external oxide scale was mainly TiO_2 and Cr_2O_3, which is in accordance with the XRD results. The distribution of Ti was saddle-shaped, that is to say that it was enriched at both the gas/solid and oxide/metal interfaces. The main elements for the internal oxide were O and Al, suggesting the internal oxide was mostly composed of Al_2O_3. Although there are oxide slightly rich in Al at the interface of external scale and the metal, continuous Al_2O_3 film was not found in the external scale according to the element distribution in Figure 7. The Ni and Co contents were both fairly low in the scale.

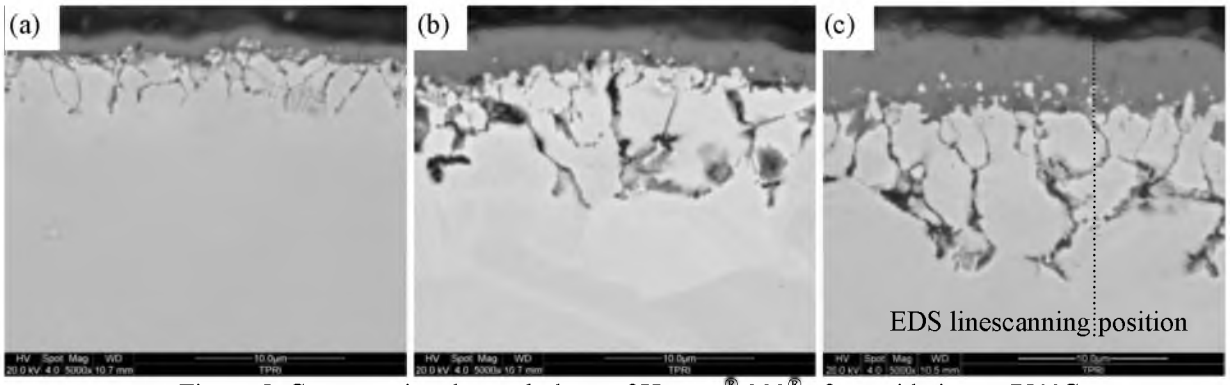

Figure 5 Cross-sectional morphology of Haynes® 282® after oxidation at 750°C
(a) 100h, (b) 1000h, (c) 2000h

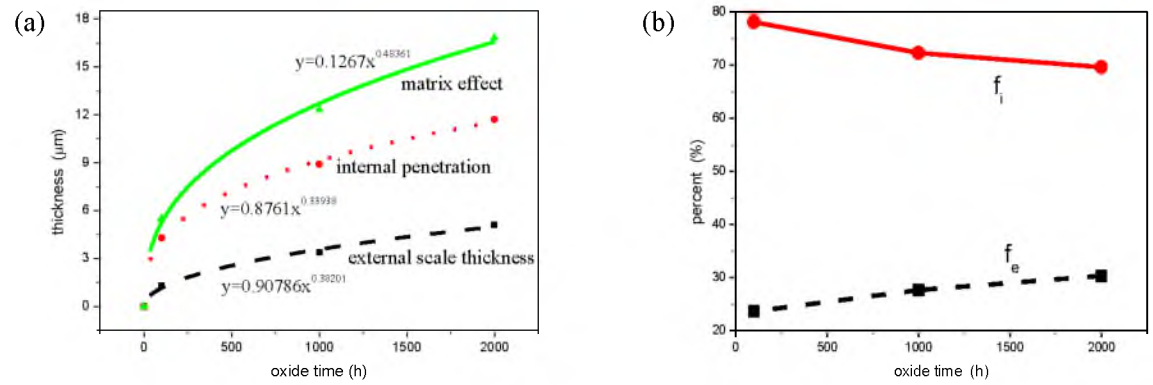

Figure 6 Oxidation kinetic curves (a) and f_i and f_e (b)

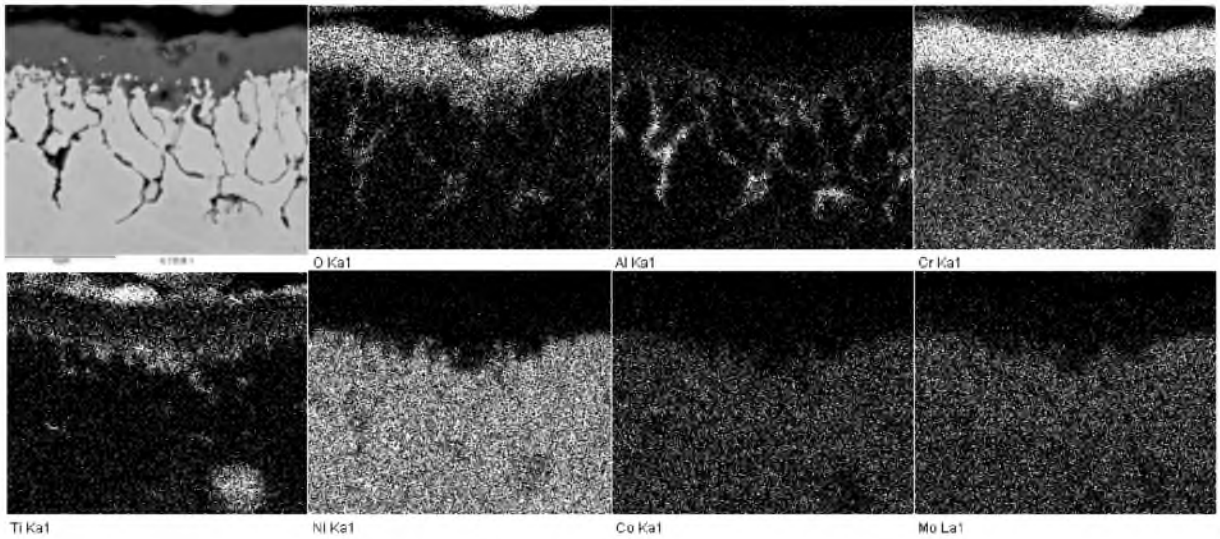

Figure 7 Element distribution maps of the scale after steam oxidation at 750°C for 2000 hours

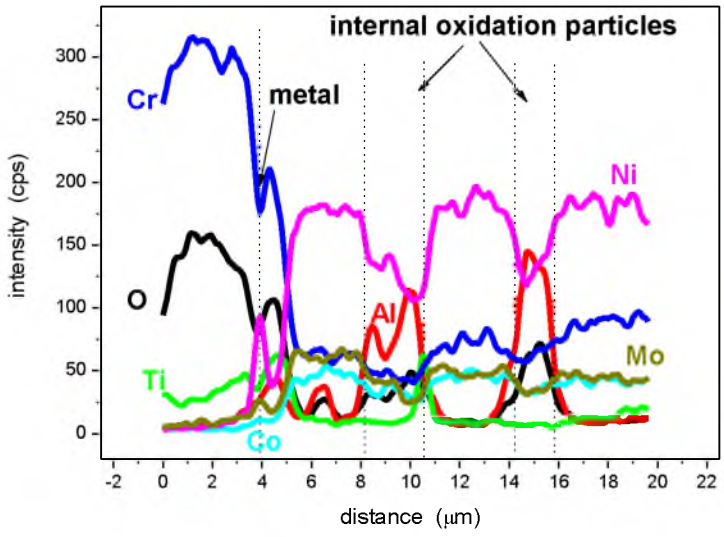

Figure 8 EDS line scanning of the scale after steam oxidation at 750°C for 2000 h

In this paper, it was found that the oxide scale of Haynes® 282® in steam was composed of a TiO_2 + Cr_2O_3 external scale and an Al_2O_3 internal subscale. TiO_2 grains in the external layer were fairly fine in the early oxidation; however, they grew up soon and connected with each other afterwards. The TiO_2 content increased obviously with oxidation time.

Ti is one of the most important elements to strengthen high temperature superalloys, which can form γ' phase with Ni, so as to improve the high temperature strength of alloys. Because the affinity of Ti to oxygen is higher than that of Cr, TiO_2 is more liable to form than Cr_2O_3. According to the XRD analysis, TiO_2 in the scale of Haynes® 282® after oxidation in steam has a rutile structure. Rutile is a kind of n-type metal oxide semiconductor (MOS), and it is usually lack of O. Rutile structure is quadrangle, of which each unit cell consists of two Ti cations and four O anions, Ti cation is in the octahedron composed of six O anions, whose coordination number with oxygen is 3. When the octahedron slightly deforms, a channel will form which allows the ions or atoms diffuse more easily. So TiO_2 is usually believed to be less protective.

TiO_2 has gained wide attention and has been researched as a semiconductor photocatalytic material. TiO_2 has super hydrophilicity, namely, the contact angle of water is less than 1^o for TiO_2 film under UV irradiation or heat treatment of higher than 400°C [17-19]. The reason is the surface of TiO_2 can promote adsorption and decomposition of H_2O. H_2O is prior to decompose into a free H atom and an OH^- ions on the (110) crystal plane of TiO_2, as shown in Figure 9 [20, 21]. The OH^- ions are also believed to introduce surface defects. A Zeller et al. studied the effect of water vapor on the oxidation behavior of γ-TiAl alloy at 700°C, and found that water vapor can lead to a significantly higher oxidation rate; meanwhile it can also change the crystalline morphology and microstructure of the oxide scale [22]. It is believed that water molecules can react with the rutile thus change its defect structure, which can change the oxidation mechanism. The studies on the oxidation behavior of TiAl alloy have shown that the diffusion rate of H in rutile is faster for 4 ~ 5 orders than that in the α-Al_2O_3 in magnitude [23, 24].

The existence of TiO_2 will destroy the integrity of the protective Cr_2O_3 film, thus lead to a worse oxidation resistance. A main idea to improve the high temperature oxidation resistance of TiAl alloy is to promote the formation of a continuous, dense and protective Al_2O_3 film, and to inhibit the formation of TiO_2 [25], which can also be used for Haynes® 282® to further improve its oxidation resistance in steam.

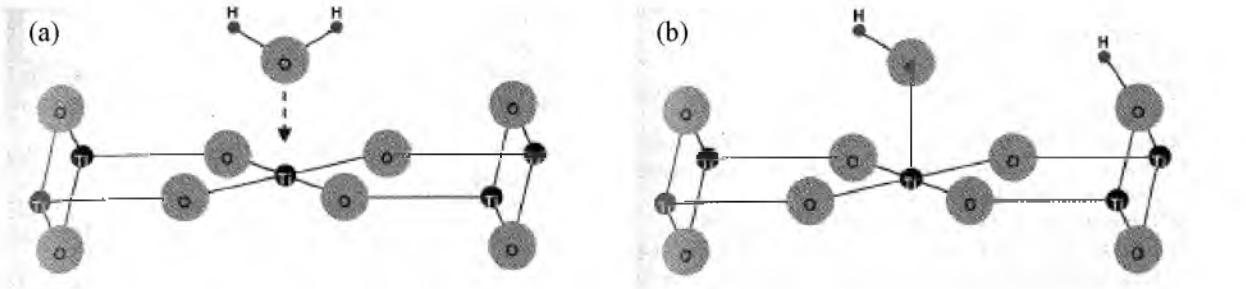

Figure 9 Two step adsorption process diagram of H_2O on the (110) crystal plane of Rutile [23]
(a) Adsorption and (b) Decomposition

Conclusion

The oxidation behavior of Haynes® 282® was investigated in steam at 750°C for up to 2000 hours. The microstructure, phase constitutes and element distribution of the oxide scale was

investigated. The oxide scale of Haynes® 282® in steam was composed of a TiO_2 + Cr_2O_3 external scale and an Al_2O_3 internal subscale. TiO_2 grains grew up and connected with each other during the oxidation, and the TiO_2 content increased obviously with oxidation time. Ti was enriched both at the gas/solid and oxide/metal interfaces. TiO_2 is believed to be harmful to the oxidation resistance of Haynes® 282® in steam due to its promotion of the adsorption and decomposition of H_2O as well as the higher diffusion rate of H in it.

Acknowledgment

This work was financially supported by the National Basic Research Program of China (973 Program, 2012CB724401), and National High-Tech Research and Development Program of China (863 Program, 2012AA050501).

Reference

[1] Bugge J, Kjær S, Blum R. High-efficiency coal-fired power plants development and perspectives [J].Energy，2006，31 (10):1437－1445.

[2] Roster J，Gotting M，Del Genovese D，et al. Wrought Ni-base superalloys for steam turbine applications beyond 700°C [J].Advanced Engineering Materials，2005，5(7)：469-483.

[3] C. DavidTung and C. John Lippold, Proc of the12th International Symposium on Superalloys, SevenSprings, PA，US, 2012.Sept. 9-13,

[4] J. Bratberg, H. Mao, L. Kjellqvist, A. EngstrÖm, P.Mason and Q. Chen, Proc of the 12th International Symposium on Superalloys, Seven Springs, PA, US, Sept. 9—13, 2012.

[5] Powell C. A., Morreale B. D.: Materials challenges in advanced coal conversion technologies, MRS Bull, 2008, 33(4), 309-315

[6] Viswanathan T., Henry J.F., Tanzosh J. et al., US program on materials technology for ultra-supercritical coal power plants, J. Mater. Eng., 2005, 14(3), 281-292

[7] Andersson J., Weldability of Precipitation Hardening Superalloys—Influence of Microstructure. Ph.D. Dissertation, Chalmers University of Technology Göteborg, Göteborg, Sweden, 2011.

[8] Pike L.M., Long Term Thermal Exposure of Haynes® 282® Alloy. In Proceedings of the 7th International Symposium on Superalloy 718 and Derivatives, Pittsburgh, PA, USA, 10–13 October 2010; Ott, E.A., Groh, J.R., Banik, A., Dempster, I., Gabb, T.P., Helmink, R.,Liu, X., Mitchell, A., Sjöberg, G.P., Wusatowska-Sarnek, A., Eds.; The Minerals, Metals andMaterials Society: Warrendale, PA, USA, 2010; pp. 645–660.

[9] Pike L.M., Development of a Fabricable Gamma-prime (γ') Strengthened Superalloy. In Proceedings of The 11th International Symposium on Superalloys, Champion, PA, USA, 14–18 September 2008; Reed, R.C., Green, K.A., Caron, P., Gabb, T.P., Fahrmann, M.G., Huron, E.S., Woodard, S.A., Eds.; The Minerals, Metals and Materials Society: Warrendale, PA, USA, 2008; pp. 191–200.

[10] Sobczak N.; Pirowski Z.; Purgert R.M.; Uhl W.; Jaskowiec, K.; Sobczak, J.J. Castability of HAYNES® 282® Alloy. In Proceeding of Workshop "Advanced Ultrasupercritical Coal-Fired Power Plants", Vienna, Austria, 19–20 September 2012.

[11] Jablonski P.D.; Hawk J.A.; Cowen, C.J.; Maziasz P.J. Processing of advanced cast alloys for A-USC steam turbine applications. J. Miner. Metals Mater. Soc. 2012, 64, 271–279.

[12] Holcomb G.R.; Jablonski P.D.; Wang P. Cast Alloys for Advanced Ultra Supercritical Steam Turbines. In Proceedings of the 7th International Symposium on Superalloy 718 and Derivatives, Pittsburgh, PA, USA, 10–13 October 2010; Ott, E.A., Groh, J.R., Banik, A., Dempster, I., Gabb, T.P., Helmink, R., Liu, X., Mitchell, A., Sjöberg, G.P., Wusatowska-Sarnek, A., Eds.; The Minerals, Metals and Materials Society: Warrendale, PA, USA, 2010; pp. 947–960.
[13] Andersson J.; Sjöberg G.; Chaturvedi M. Hot Ductility Study of HAYNES® 282® Superalloy. In Proceedings of the 7th International Symposium on Superalloy 718 and Derivatives, Pittsburgh, PA, USA, 10–13 October 2010; Ott, E.A., Groh, J.R., Banik, A., Dempster, I., Gabb, T.P., Helmink, R., Liu, X., Mitchell, A., Sjöberg, G.P., Wusatowska-Sarnek, A., Eds.; The Minerals, Metals and Materials Society: Warrendale, PA, USA, 2010; pp. 539–554
[14] Haynes International, Inc. HAYNES® 282® ALLOY, material data sheet. Available online: http://www.christianberner.se/$-1/file/filarkiv/cbab/dokument/legeringar-pdf-dokument/haynes-282-alloy.pdf (accessed on 22 September 2005).
[15] P.F. Tortorelli, K.A. Unocic, H. Wang, M.L. Santella, Creep-Rupture Behavior Of Precipitation-Strengthened Ni-Based Alloys Under Advanced Ultra-supercritical Steam Conditions
[16] Vinay P. Deodeshmukh, and Nacéra Sabrina Meck. High-Temperature Oxidation Resistance Of Solid-Solution And Gamma prime Strenghthened Alloys In The Presence Of Water Vapor, NACE International, Corrosion 2011 Conference & Expo, Paper No. 11195
[17] R. Wang, K. Hashimoto, A. Fujishima, M. Chikuni, E. Kojima, A. Kitamura, M. Simohigoshi, T. Watanabe, Light-induced amphiphilic surfaces, Nature, 1997, 388: 431-432
[18] R. Wang, K. Hashimoto, A. Fujishima, M. Chikuni, E. Kojima, A. Kitamura, M. Simohigoshi, T. Watanabe, Photogeneration of Highly Amphiphilic TiO_2 Surfaces, Advanced Materials, 1998, 10(2): 135-138
[19] R. D. Sun, A. Nakajima, A. Fujishima, T. Watanabe, K. Hashimoto, Photoinduced surface wettability conversion of ZnO and TiO_2 thin films, J. Phys. Chem. (B), 2001, 105: 1984~1990
[20] Bredow T, Jug K. Surface Science, 1995, 327:398
[21] Henderson MA. Surface Science 1996; 355: 151
[22] Zeller A, Dettenwanger F, and Schütze M.. Influence of water vapour on the oxidation behaviour of titanium aluminides[J]. Intermetallics, 2002,10(1): 59–72.
[23] Fowler JD, Chandra D, Elleman TS, Payne AW, Verghese K. J AM Ceram Soc, 1997, 60:155
[24] Johnson OW, Paek SH, DeFord JW. J Appl Phys, 1975, 46: 1026
[25] Peng Xiaomin, Xia Changqing, Wang Zhihui. Development of high temperature oxidation and protection of TiAl-based alloy[J]. The Chinese Journal of Nonferrous Metals. 2010, 20(6):1116-1130